Photobiomodulation, Photomedicine, and Laser Surgery
Volume 38, Number 5, 2020

Pp. 301–307
DOI: 10.1089/photob.2019.4724

Method for Accurately Preparing Cavities on Cortical Bones Using Picosecond Laser

Shanshan Liang, PhD,[1–6] Peijun Lyu, PhD,[1–6] and Fusong Yuan, PhD[1–6]

Abstract

Objective: This study was conducted to (1) evaluate a new method for accurately and automatically preparing dental implant cavities; (2) investigate the quantitative relationships between the number of focal-plane additive pulse layers (n) in two-dimensional ablation, the Z-axis feed rate, and the ablation depth (d) during cortical-bone ablation using a numerically controlled three-axis picosecond laser; and (3) establish appropriate methods for precise ablation control.

Materials and methods: Two-dimensional ablation was performed on swine-rib blocks in the focal plane on a preset circular path using a picosecond laser device and an in-house-developed three-axis numerically controlled micro-laser galvanometer scanner. The maximum two-dimensional d and the quantitative relationship between n and d within the maximum d were consequently obtained. The measured and theoretical values of the ablated cavities were then compared to obtain n and d values corresponding to the minimum difference, and to evaluate the error in d, resulting in a higher-accuracy d value (i.e., single-step ablation depth) being obtained.

Results: The diameter and deep errors between the measured and design data for 24 cavities were 2.76 ± 1.51 and 10.23 ± 4.82 μm, respectively. Thus, high-quality cortical-bone cavities preparation was achieved using a picosecond laser with the parameters employed in this study.

Conclusions: Precise control of cortical-bone ablation using a picosecond laser can be attained by optimizing the single-step ablation parameters.

Keywords: laser in dentistry, bone, implants, laser surgery

Introduction

SINCE 1964, LASERS have been applied in the field of stomatology, promoting the rapid development of stomatological technology. To date, laser technology has pervaded various disciplines of stomatology, including basic and applied research; diagnosis and treatment of oral mucosal and periodontal diseases; dentin hyper sensitivity treatment; control of dental caries and removal of carious tissue; and hard tissue removal and sterilization during cavity and tooth preparation.

As a result, commercial laser devices have emerged that possess distinct advantages for soft-tissue disease treatment. However, such devices have the following limitations as regards removal of the hard tissue of the teeth and jaw: (1) difficulty achieving precise control; (2) risk of thermal and mechanical damage to the remaining tissue; (3) lower ablation efficiency for air-cooled, water-cooled, or higher-repetition frequency lasers than that for conventional drilling.[1,2]

To realize the potential of new laser applications in stomatology, researchers worldwide have studied the plasma effect produced during laser ablation of hard tissue.[3,4] It has been found that, with appropriate parameters, picosecond lasers can overcome the current defects of commercial stomatological laser devices or even outperform those devices. In particular, the results of a previous study[5] have shown that ultrashort pulse lasers are superior to conventional mechanical grinding technology or other long- and short-pulse lasers for ablation of the hard tissue of the teeth and jaw. The major advantages are as follows: (1) high

[1]Centre of Digital Dentistry, Peking University School and Hospital of Stomatology, Beijing, China.
[2]Department of Prosthodontics, Peking University School and Hospital of Stomatology, Beijing, China.
[3]National Engineering Laboratory for Digital and Material Technology of Stomatology, Beijing, China.
[4]Research Centre of Engineering and Technology for Digital Dentistry of Ministry of Health, Beijing, China.
[5]Beijing Key Laboratory of Digital Stomatology, Beijing, China.
[6]National Clinical Research Center for Oral Diseases, Beijing, China.

ablation efficiency; (2) considerable reduction of mechanical and thermal damage; (3) higher-precision ablation control; (4) low noise; (5) pain reduction; (6) surface texture adjustment capability through control of the laser beam shape and grating; (7) precise control and improved safety (intensity-dependent multi-photon processing ensures that tissue below and around the focal spot is not ablated by the laser); (8) effective ablation of all tissue types through a nonlinear action mechanism.[6] Recent studies on high-energy and high-repetition frequency lasers have allowed exploitation of these advantages.[7,8]

At present, research on the application of ultrashort pulse lasers to dental hard tissue is focused on microscopic morphology, the temperature effect, and ablation efficiency.[9,10] In recent years, Yuan et al. have commenced relevant studies on precise control in dental hard tissue.[11]

The present study was primarily conducted to analyze the quantitative relationship between the number of laser scanning layers (n) and the ablation depth (d) for the case of cortical-bone ablation performed using a picosecond laser. The results were subsequently used to determine an optimized Z-axis feed rate for a numerically controlled picosecond laser, so as to achieve precise control of the cortical-bone d; this finding will provide a solid foundation for subsequent studies on automated implant surgery using a numerically controlled picosecond laser.

Materials and Methods

Equipment and software

The laser system employed in this study was a picosecond laser device (wavelength: 1064 nm, pulse width: 15 ps, repetition frequency: 100 kHz, power: 30 W, laser focal spot: 38 μm diameter, energy per pulse: 300 μJ, energy density: 2.647×10^{-3}J/cm^2) (Table 1). Note that the focal spot diameter was derived from a charge coupled device (CCD) measurement conducted when the laser was focused on the surface of the tooth to be ablated through a 175-mm lens. A numerically controlled laser scan system was employed, that is, an in-house-developed micro-laser tooth body preparation intraoral working device, with the following specifications: focal spot scanning speed for two-dimensional scanning galvanometer: 1900 mm/s; minimum step size along Z-axis: 0.1 mm; maximum step size: 10 mm. The numerical control software was developed in-house. The sample-stage position control device was a spiral micrometer (Mitutoyo Corporation, Japan; precision: 0.01 mm) and the three-dimensional measuring device was a three-dimensional laser scanning microscope (VK-X200; Keyence Corporation, Japan). Air cooling machine [DXW50; Denair Energy Saving Technology (Shanghai) PLC, China] was used in the experiment.

The reverse engineering software packages used in this study were Geomagic software (Studio and Qualify 2012, 3D Systems, Inc., Rock Hill, SC), and Imageware (13.1, Siemens PLM Software, Berlin, Germany).

Sample preparation

Eight fresh left and right ribs (from first rib to fourth rib) of a single 7-month-old healthy pig were obtained from a certified official slaughter house. Although pig ribs are weaker than the human mandible, they are excellent in homogeneity of the thickness of cortical bone. The soft tissue on the rib surface was removed and the ribs were rinsed with normal saline. The ribs were then cut into 16 blocks with 5 cm lengths using a diamond wire saw (STX-202; Shenyang Ke jing Auto-instrument Co. Ltd.). For each block, the sides with relatively uneven surfaces were enclosed in silicone rubber to form even surfaces, while the relatively even surface was designated as the surface for ablation. The surface for ablation was polished sequentially using 800-, 1000-, and 2000-grit waterproof sandpaper to form an essentially flat surface. The rib specimens were then immersed in formalin solution (10%, Leagene; Anhui Leagene Biotechnology Co., Ltd.) until use. The whole experiment lasted about 8 h.

This investigation was approved by Biomedical Ethics Committee of Peking University (No. LA2017281).

Two-dimensional scanning and ablation

One swine-rib block was mounted on a sample stage, which was mounted on a movable platform with spiral micrometers. That is, the two-dimensional movements of the platform were controlled by two spiral micrometers. The picosecond laser beam was oriented perpendicular to the ablation surface, and the platform was adjusted with the spiral micrometers so as to position the ablation surface at the focal point in front of the lens center. The laser path was modeled computationally (Figs. 1 and 2) and laser scanning was

Table 1. Report Parameters in Experimental Laser Device

Manufacturer	Academy of Opto-Electronics, Chinese Academy of Sciences
Model identifier	GK-1064
Year produced	2013
Number and type of emitters (laser or LED)	Picosecond laser
Wavelength and bandwidth (nm)	1064
Pulse mode (CW or Hz, duty cycle)	100 KHz
Beam spot size at target (cm^2)	1.134×10^{-13}
Irradiance at target (mW/cm^2)	2.646×10^{17}
If pulsed peak irradiance (mW/cm^2)	3.527×10^{17}
Exposure duration (sec)	15 psec
Energy density (J/cm^2)	2.647×10^{-3}
Radiant energy (J)	3×10^{-4}
Area irradiated (cm^2)	7.069×10^{-6}
Number and frequency of treatment sessions	Complete the treatment in 1 day

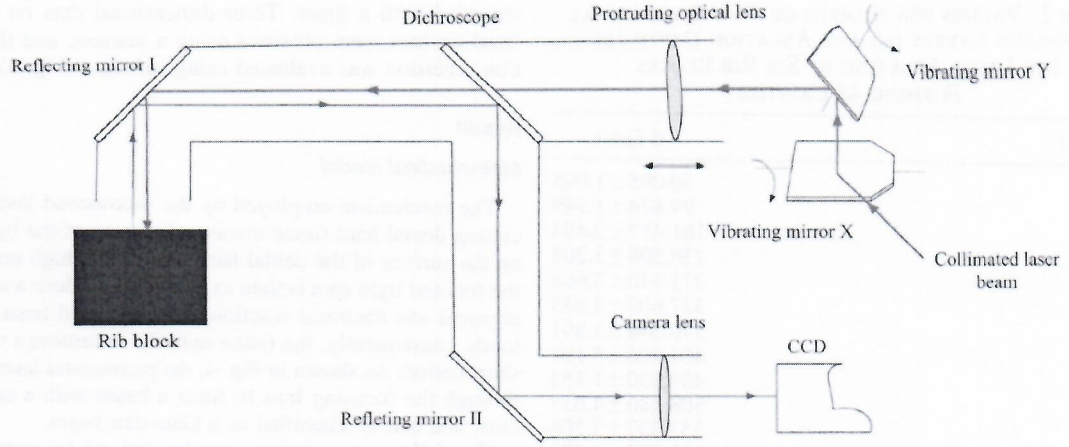

FIG. 1. Schematic diagram of experimental platform.

performed along the modeled motion path, with the space between frames set to 19 μm (50% overlap rate). The rib block and lens positions were kept unchanged for subsequent ablation by the picosecond laser along the motion path for 5 n. Recall that one layer (n) denotes the completion of one ablation motion from the outer to inner frame by the laser. Thereafter, the spiral micrometers were used to position the next ablation site. Different ablation sites were scanned for $n=5$, 10, 15, 20, 25, 30, 35, and 40, yielding eight circular cavities with 3-mm diameter and varying depths. The same process was performed on another rib block, with ablation sequentially performed for $n=45$, 50, 55, 60, 65, 70, 75, and 80, to form another eight circular cavities with 3-mm diameter and varying depths. This process was repeated three times.

Measurement of two-dimensional d

The actual d of each circular cavity was measured using a three-dimensional shape-measurement laser microscope. Twenty points at the base of each ablated circular cavity were chosen (these points were distributed as evenly as possible on the cleaved surface). With the upper surface as a reference, the depths of the 20 points were measured individually to calculate the mean value, which represented the d for each layer. The mean d was then calculated from the d values at the same layer for three rib blocks, so as to derive the maximum d value for cortical-bone ablation by the laser without Z-axis feed motion. A curve of the quantitative relationship between d and n was then plotted.

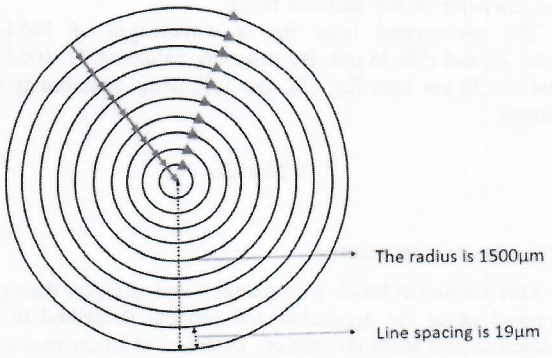

FIG. 2. Two-dimensional motion paths of ultrashort pulse laser—similar to a concentric circular motion in the plane. The larger red arrows represent the circular motion of the laser, and the smaller red arrows indicate the direction of the laser from the outer ring to the inner ring.

Three-dimensional scanning and ablation

One rib block was mounted on the sample stage. The spiral micrometers were used to orientate the sample stage toward the laser incidence direction, so that the ablation surface was oriented perpendicular to the main axis of the laser beam and superimposed on the focal plane of the laser. Parameters such as the focal plane two-dimensional scanning path were set as described in the Two-Dimensional Scanning and Ablation section. The timing for stepwise increments along the normal was set for n at 1–0 layers (in steps of one). The single step size was set according to the relation $d=9.1255n+34.664$, which was obtained from linear regression analysis of the quantitative relationship between d and n. The number of steps, t, was set to 45, 36, 31, 27, 24, 21, 19, 17, 16, and 14. Ten square cavities (4×2 mm) were cut into two rib blocks (each block had five cavities). This was repeated three times. The n for stepwise increments along the Z-axis was set to 1, 2, 3, 4, 5, 6, 7, 8, 9, and 10. The single-step size was obtained from the integer value of the corresponding two-dimensional d values. For each setup, three-dimensional scanning was performed on the ablation surface to form a circular cavity with a 4-mm diameter. The n values, single-step d values, number of steps, and theoretical d values are listed in Table 2.

Measurement of three-dimensional ablation d

A three-dimensional laser shape measurement microscope was used to measure the actual total ablation depth, d_2, of each circle cavity by using the method described in the Measurement of Two-Dimensional d section. The theoretical total ablation depth is $d_1=d_0\times(t+1)$, where d_0 is the theoretical single step ablation depth. The relationships among e, n, and d were analyzed.

TABLE 2. VALUES FOR NUMBER OF TWO-DIMENSIONAL SCANNING LAYERS (*N*) AND ABLATION DEPTH (*D*) FOR LASER ABLATING OF SIX RIB BLOCKS FORMING 48 CAVITIES

n *(layer)*	d *(μm)*
5	50.095 ± 1.095
10	99.874 ± 1.949
15	161.417 ± 2.494
20	230.508 ± 3.205
25	272.440 ± 3.666
30	327.609 ± 4.635
35	370.544 ± 3.891
40	404.906 ± 5.197
45	459.830 ± 1.852
50	508.286 ± 4.637
55	553.337 ± 5.206
60	603.579 ± 3.400
65	633.853 ± 3.554
70	654.938 ± 3.443
75	663.980 ± 2.887
80	663.249 ± 2.462

Acquisition of single-step d *and measurement of ablation precision*

From the procedure described for measurement of three-dimensional *d* values, the optimum *n* for a single-step increment along the Z-axis was determined to be one. One rib block was mounted on the sample stage. Again, the spiral micrometers were used to orientate the sample stage toward the laser incidence direction, so that the ablation surface was oriented perpendicular to the main axis of the laser beam and superimposed on the laser focal plane. The two-dimensional scanning pathway in the focal plane was as follows: Laser scanning was performed from top to bottom to generate five concentric circles of increasing diameter, with five pulse layers for each concentric circle. The convex lens was kept stationary during the entire scanning process. Three-dimensional scanning was subsequently performed with a three-dimensional shape-measurement laser microscope, and the vertical depths of adjacent concentric circles were measured. Finally, the mean cortical-bone *d* obtained using $n = 1$ was calculated and set as the single-step *d*. This depth was used to determine the Z-axis feed rate for the ablation of cylindrical cavities having 4-mm diameter and 3-mm depth. The ablation time of each cylindrical cavity was recorded with a timer. Three-dimensional data on the ablated cavities were obtained using a scanner, and the ablation precision was evaluated using software (Fig. 3).

TABLE 3. PARAMETER SETTINGS AND RESULTS FOR THREE-DIMENSIONAL RIB-BLOCK ABLATION

n *(layer)*	d_0 *(μm)*	t *(time)*	d_1 *(μm)*	d_2 *(μm)*	e *(μm)*
1	43	45	1978	1976.15	1.85
2	53	36	1961	1957.94	3.06
3	62	31	1984	1977.69	6.31
4	71	27	1988	1977.86	10.14
5	80	24	2000	1986.73	13.27
6	89	21	1958	1944.11	16.89
7	99	19	1980	1954.84	25.16
8	108	17	1944	1909.41	34.59
9	117	16	1989	1937.63	51.37
10	126	15	2016	1943.47	72.53

Result

Mathematical model

The mechanism employed by the picosecond laser when cutting dental hard tissue involves focusing of the light spot on the surface of the dental hard tissue. The high energy of the focused light spot is then exploited to produce a series of physical and chemical reactions with the hard tissue of the tooth; consequently, the tissue material is removed within a short period. As shown in Fig. 4, the picosecond laser passes through the focusing lens to form a beam with a small radius, and can be classified as a Gaussian beam.

The following equations can be derived by considering the Gaussian-beam focusing principle:

$$\omega'_0 = \frac{\lambda}{\pi\omega(z)} f, \tag{1}$$

$$Z_R = \frac{\pi\omega'^2_0}{\lambda}, \tag{2}$$

where $\omega(z)$ is the section radius of the incident Gaussian beam, which is related to the propagation distance of the light beam; λ is the wavelength of the light beam; f is the lens focal length; ω'_0 is the waist radius of the emergent light beam; and Z_R is half the waist length of the emergent light beam, which is the effective working length for laser preparation.

When parallel light is incident on the lens, $Z \geq f'$ and the waist radius of the incident beam is $\omega(z)$. Further, the exit beam can be focused to a very small beam spot radius of ω'_0. By substituting the medical parameters into Eq. (1), the following relation is obtained:

$$d = \frac{4\lambda}{\pi D_1} f, \tag{3}$$

where d is the diameter of the focused light spot and D_1 is the diameter of the incident beam.

The picosecond laser has a wavelength of 1064 nm (i.e., λ), and d is 38 μm. By inserting values of $\lambda = 1064$ nm and $d = 30$ μm into Eq. (3), the following equation is obtained:

$$f \approx 22.14 D_1. \tag{4}$$

Two-dimensional ablation

One swine-rib block was scanned and ablation then performed using the apparatus and process described in the Materials and Methods section. Different ablation sites were created for different values of *n*; one layer (*n*) corresponds to one completed ablation motion from the outer to inner frame by the laser. A total of 16 ablation cavities (8 cavities on 2 separate blocks) with 3-mm diameter and different depths were obtained. The process was repeated three times;

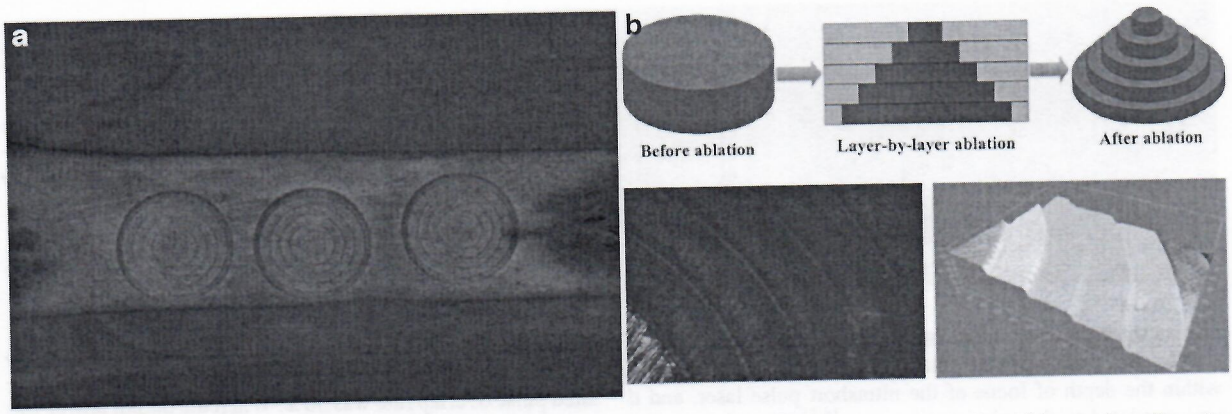

FIG. 3. Method for acquisition of single-step ablation depth. (**a**) Showing five concentric circles of increasing diameter ablated on bone. (**b**) Measuring the single-step ablation depth.

Table 1 lists the mean values and cumulative results for the d value corresponding to each n setting for laser ablation of the rib blocks. In addition, the quantitative relationship between the cortical-bone d and n was established. From this relationship, the maximum d of the cortical-bone ablation produced by the laser without Z-axis feed motion (i.e., two-dimensional ablation) was determined to be 664 ± 3 μm. The quantitative relationship between the cortical-bone d and n exhibited a linearly increasing tendency, and the functional expression and fit coefficient derived through linear fitting were $d = 9.1255n + 34.664$ $(1 \leq n \leq 75)$, with $R^2 = 0.9876$.

Three-dimensional ablation

Next, three-dimensional ablation was performed by incorporating Z-axis feed motion into the scanning and ablation process, as detailed in the Materials and Methods section. The actual d of each cavity was measured using a three-dimensional shape-measurement laser microscope (see Materials and Methods section); the differences between the theoretical and actual d values for each cavity are listed in Table 3.

Precision control during three-dimensional ablation

The mean single-step d was determined to be 43 μm, which was used to set the Z-axis feed rate for the ablation of 24 cylindrical cavities. The mean ablation time of each cylindrical cavity is about 5 min. Measurement results obtained using software showed that the errors between the measured and design data for diameter and cavities deep were 2.76 ± 1.51 and 10.23 ± 4.82 μm, respectively (Fig. 5).

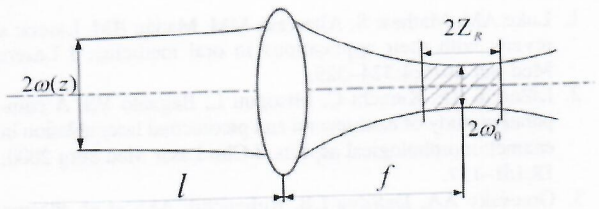

FIG. 4. Gaussian beam. $\omega(z)$: section radius of incident Gaussian beam; Z_R and ω'_0: half waist length and waist radius of emergent light beam, respectively; f: lens focal length.

The experimental results suggest that precise control can be achieved when cortical bone is ablated with a numerically controlled picosecond laser. The curve of the quantitative relationship between n and d indicates a generally positively linear relationship between these parameters during two-dimensional ablation of cortical bone, without Z-axis feed motion in the laser tooth preparation system (i.e., two-dimensional ablation with the lens kept stationary). For three-dimensional ablation of cortical bone by the picosecond laser (i.e., with automated Z-axis feed motion), the smaller the single-step increment, the more precise the ablation control. When the n for a single-step increment along the Z-axis was set to one, the ablation depth precision could be controlled with an error of 1.85 μm.

Conclusions

Precise control of cortical-bone ablation using a picosecond laser can be attained by optimizing the single-step ablation parameters. And, the dental implant cavity can be automatically prepared using the method.

Discussion

Since the 1960s, researchers worldwide have investigated laser application in stomatology, with the long-term goal of developing an advanced laser system that can replace the air-turbine dental handpiece. In recent decades, studies on laser application in stomatology have revealed that the action of ultrashort pulse lasers on dental hard tissue mainly manifests as plasma-induced ablation, which is caused by plasma ionization. As this process is extremely rapid, very little energy is transmitted to the surrounding tissue; therefore, little thermal damage is inflicted on that tissue.[12,13] When plasma-induced ablation is used, smooth and clearly outlined tissue dissociation surfaces with no trace of thermal or mechanical damage can be observed. Numerous studies have confirmed that precise ablation of dental hard tissue and control of thermal damage within a certain range can be achieved through use of ultrashort pulse lasers with appropriate parameters.

On the basis of the aforementioned studies, methods for the precise control of morphology and depth during ablation of bone tissue by a numerically controlled picosecond laser were explored in this work. A precise single-layer d is fundamental, and a key requirement for the achievement of

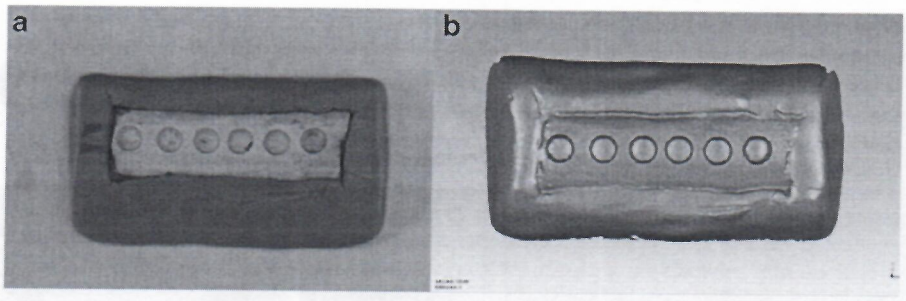

FIG. 5. Bone cavities were precisely ablated. (**a**) Showing bone cavities ablated. (**b**) 3-D model of bone cavities.

precise three-dimensional ablation of bone tissue. In previous studies, three-dimensional ablation could only be performed within the depth of focus of the ultrashort pulse laser, and d was restricted to the micrometer range.[14,15] Therefore, applications in common bone tissue surgeries in the clinical practice of stomatology were impossible. In this experiment, a picosecond laser with specific parameters (including power, repetition frequency, focal spot diameter, and scanning speed) was used to ablate bone tissue according to a specific ablation path (different layers of concentric circles), and the single-step d of the bone tissue ablation performed by the picosecond laser was obtained. This depth was used to configure the movement of the focal plane to ensure superposition of the ablation surface on the focal plane throughout the entire process. Hence, d values in the millimeter range were achieved; this satisfies the requirement for clinical bone tissue surgeries. In this experiment, d was controlled to within the cortical-bone thickness, primarily to avoid the effects of material heterogeneity and bleeding. Hence, the feasibility of the employed methods was validated. In subsequent studies, d will be extended downward to the cancellous bone, and the effects of material heterogeneity and bleeding will be the main focal points of that investigation. In this study, three-dimensional measurement of the depth of ablation cavities in vitro was performed using a surface 3D scanner and software, and the accuracy controlled in the micron range. However, the measurement method cannot be applied to the ablation cavities of intravital tissue. The development of Optical Coherent Tomograph (OCT) technology will provide us with new measurement methods. A survey of the literature available shows that the technology has been applied to the fields of ophthalmology, dermatology, and so on. For intravital tissue, the measurement accuracy can be controlled in the micrometer range.[16–19] In future research, OCT technology will be further studied and applied to the field of stomatology.

Different laser parameters such as surface scanning speed, repetition frequency, output power, and wavelength can cause lasers to have different effects on bone tissue, which may result in carbonization and temperature increase (from 5°C to 100°C). This suggests that repetition frequency has an important influence on the laser ablation process. The higher the repetition frequency, the more likely is the occurrence of carbonization on the bone tissue surface and a temperature increase. In contrast, low repetition frequency yields less thermal damage. In a study by Gill et al.,[20] it was found that an increase in the repetition frequency of a 40-J/cm^2 femtosecond laser from 1 to 20 kHz yields a temperature increase of 2°C–40°C and carbonization. In addition, the focal spot diameter has an impact on the pulse overlap rate. In this experiment, the focal spot diameter of the picosecond laser measured via a CCD was $\sim 38\ \mu$m, repetition frequency was 100 kHz, scanning speed was set to 1900 mm/s, and calculated pulse overlap rate was 50%. When the output power was adjusted to 30 W, relatively good performance was achieved for the laser ablation of cortical bone and no carbonization occurred. Subsequent experiments will be performed to investigate the degree of temperature increase during ablation. In this study, we chose the 1064 nm picosecond laser, because it could achieve precise cutting of hard tissues and can reduce heat production, according to reports in the literature.[12] Jowett et al. researched picosecond infrared laser ablation of soft tissue, cartilage, and bone tissue, and obtained results indicating that no thermal damage and mechanical damage occurred during the soft tissue, cartilage, and bone tissues ablation by the picosecond laser at this wavelength.[21]

Moreover, with the continuous advancement of technology and the continuous deepening of laser research, lasers are being increasingly more widely used in medicine. A modern laser-processing strategy gives us an idea of laser application. Esteves-Oliveira et al.[22] found a combination of laser parameters to automatically ablate the enamel surface that could cause a temperature increase of over 600°C at the enamel surface while not damaging the enamel, avoiding temperature change above 5.5°C in the pulp, and increasing enamel erosion resistance.

Author Disclosure Statement

No competing financial interests exist.

Funding Information

This study was supported by the National Natural Science Foundation of China (grant no. 81571023), the Clinical Medicine Plus X - Young Scholars Project of Peking University (grant no. PKU2019LCXQ024), and the State Key Lab of Advanced Metals and Materials (grant no. 2018-Z04).

References

1. Luke AM, Mathew S, Altawash MM, Madan BM. Lasers: a review with their applications in oral medicine. J Lasers Med Sci 2019;4:324–329.
2. LiZarelli RF, Kurachi C, Misoguti L, Bagnato VS. A comparative study of nanosecond and picosecond laser ablation in enamel: morphological aspects. J Clin Laser Med Surg 2000; 18:151–157.
3. Oraevsky AA, DaSilva LB, Rubenchik AM, et al. Plasma mediated ablation of biological tissues with nanosecond-to-femtosecond laser pulses: relative role of linear and nonlinear absorption. IEEE J Sel Top Quant Electron 1996;2: 801–809.

4. Lo DD, Mackanos MA, Chung MT, et al. Femtosecond plasma mediated laser ablation has advantages over mechanical osteotomy of cranial bone. Lasers Surg Med 2012; 44:805–814.4
5. Neev J, Silva LBD, Feit MD, Perry MD. Ultrashort pulse lasers for hard tissue ablation. IEEE J Sel Top Quantum Electron 1996;2:790–800.
6. Esteves-Oliveira M, Jansen P, Wehner M, et al. Surface characterization and short-term adhesion to zirconia after ultra-short pulsed laser irradiation. J Adhes Dent 2016;18: 483–492.
7. Sun YC, Yuan FS, Lv PJ, Wang DX, Wang L, Wang Y. Method to control depth error when ablating human dentin with numerically controlled picosecond laser: a preliminary study. Lasers Med Sci 2015;30:1435–1441.
8. Yuan FU, Zheng JQ, Sun YU, Wang Y, Lyu PJ. Regulation and measurement of the heat generated by automatic tooth preparation in a confined space. Photomed Laser Surg 2017;35:332–337.
9. Braun A, Krillke RF, Frentzen M, Bourauel C, Stark H, Schelle F. Heat generation caused by ablation of dental hard tissues with an ultrashort pulse laser (USPL) system. Lasers Med Sci 2015;30:475–481.
10. De Menezes RF, Harvey CM, de Martínez Gerbi MEM, et al. Fs-laser ablation of teeth is temperature limited and provides information about the ablated components. J Biophotonics 2017;10:1292–1304.
11. Yuan FS, Lyu PJ, Wang DX, Wang L, Sun YC, Wang Y. Controlling dental enamel-cavity ablation depth with optimized stepping parameters along the focal plane normal using a three axis, numerically controlled picosecond laser. Photomed Laser Surg 2015;33:92–97.
12. Bello-Silva MS, Wehner M, Eduardo Cde P, et al. Precise ablation of dental hard tissues with ultra-short pulsed lasers. Preliminary exploratory investigation on adequate laser parameters. Lasers Med Sci 2013;28:171–184.
13. Rode AV, Gamaly EG, Luther-Davies B, et al. Precision ablation of dental enamel using a subpicosecond pulsed laser. Aust Dent J 2003;48:233–239.
14. Lim YC, Altman KJ, Farson DF, Flores KM. Micropillar fabrication on bovine cortical bone by direct-write femtosecond laser ablation. J Biomed Opt 2009;14:064021.
15. Liu Y, Niemz M. Ablation of femural bone with femtosecond laser pulses—a feasibility study. Lasers Med Sci 2007;22:171–174.
16. Luigina S, Jyotsna M, Katrin M. Use of the Visante™ OCT to measure the sagittal depth and scleral shape of keratoconus compared to normal corneae: Pilot study. J Opto 2013;6:141–146.
17. Vermeer KA, Mo J, Weda JJ, Lemij HG, de Boer JF. Depth-resolved model-based reconstruction of attenuation coefficients in optical coherence tomography. Biomed Opt Express 2013;5:322–337.
18. Varkentin A, Mazurenka M, Blumenröther E, et al. Comparative study of presurgical skin infiltration depth measurements of melanocytic lesions with OCT and high frequency ultrasound. J Biophotonics 2017;10:854–861.
19. Waibel JS, Rudnick AC, Wulkan AJ, Holmes JD. The diagnostic role of optical coherence tomography (OCT) in measuring the depth of burn and traumatic scars for more accurate laser dosimetry: Pilot study. J Drugs Dermatol 2016;15:1375–1380.
20. Gill RK, Smith ZJ, Lee C, Wachsmann-Hogiu S. The effects of laser repetition rate on femtosecond laser ablation of dry bone: A thermal and LIBS study. J Biophotonics 2016;9:171–180.
21. Jowett N, Wöllmer W, Reimer R, et al. Bone ablation without thermal or acoustic mechanical injury via a novel picosecond infrared laser (PIRL). Otolaryngol Head Neck Surg 2014;150:385–393.
22. Esteves-Oliveira M, Wollgarten S, Liebegall S, et al. A new laser-processing strategy for improving enamel erosion resistance. J Dent Res 2017;96:1168–1175.

Address correspondence to:
Fusong Yuan, PhD
Center of Digital Dentistry
Peking University School and Hospital of Stomatology
22 Zhongguancun Nandajie
Haidian District
Beijing 100081
China

E-mail: yuanfusong@bjmu.edu.cn

Received: July 13, 2019.
Accepted after revision: December 5, 2019.
Published online: April 27, 2020.